J. Fluid Mech. (2024), *vol*. 987, R9, doi:10.1017/jfm.2024.369

Turbulent Couette flow up to $Re_\tau = 2000$

Sergio Hoyas[1],† **and Martin Oberlack**[2,3]

[1]Instituto de Matemática Pura y Aplicada, Universitat Politècnica de València, Camino de Vera, 46024 València, Spain

[2]Chair of Fluid Dynamics, TU Darmstadt, Otto-Berndt-Str. 2, 64287 Darmstadt, Germany

[3]Centre for Computational Engineering, TU Darmstadt, Dolivostraße 15, 64293 Darmstadt, Germany

(Received 19 November 2023; revised 29 January 2024; accepted 5 April 2024)

Two simulations of turbulent Couette flows were performed at friction Reynolds numbers of 1000 and 2000 in a large box of dimensions $L_x = 16\pi h$, $L_y = 2h$ and $L_z = 6\pi h$, where h is the semi-height of the channel. The study focuses on the differences in the intensity and scaling of turbulence at these two Reynolds numbers. The 2000 case showed a lack of a clear log layer with a higher value of the Von Kármán constant κ than Poiseuille channels. The intensities were well-scaled in the buffer layer and below, with a second maximum of the streamwise intensity at approximately 350 wall units. Contrary to Poiseuille channels, the dissipation scales close to the wall in wall units. This fact can be attributed to the constant value of the derivative of the streamwise intensity in wall units. The intensities of the 2000 case showed remarkable differences compared with those at Reynolds number 1000 at the channel centre, likely due to the organization of large scales of the streamwise fluctuactions, u. These large scales were thought to be considered 'infinite'. However, for the 2000 case, while all the structures have a width of $\ell_z \approx 6/8\pi h$, their length varies from $\ell_x \approx 6\pi h$ to $\ell_x \approx 16\pi h$, which clearly contradicts the trends obtained in the past. This is a new effect that has not been reported for turbulent Couette flow and points to the uncertainty and sensitivity that is observed for certain statistical quantities.

Key words: turbulence theory, turbulent boundary layers

1. Introduction

Direct numerical simulation (DNS) has become one of the main tools in studying wall turbulence. This fact is especially true in the case of Couette flows, which are investigated in the present study; see figure 1. The flow is confined between two parallel plates.

† Email address for correspondence: serhocal@mot.upv.es

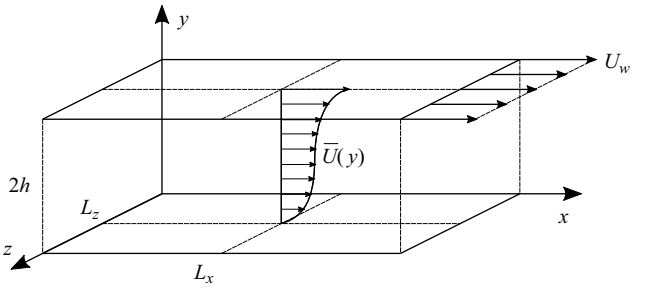

Figure 1. Sketch of plane Couette flow driven by the velocity U_w of the upper wall. The dimensions of the computational box are $L_x \times 2h \times L_z$.

The bottom plate remains stationary while the top one moves at a velocity U_∞. As in pressure-driven channels, i.e. Poiseuille flows, the main control parameter is the friction Reynolds number $Re_\tau = u_\tau h/\nu$, where u_τ is the friction velocity, ν is the kinematic viscosity, and h is the channel half-width. Since the seminal work of Kim, Moin & Moser (1987), the turbulence community focuses on plane Poiseuille flows. The value of Re_τ has increased from 180 to 10 000 in 35 years (Oberlack *et al.* 2022). However, considerably less attention has been paid to plane Couette flows. Several reasons make these flows harder to study. From an experimental point of view, the set-up with a moving wall is difficult to implement properly (Tillmark 1995). The main issue for numerical studies is the long and wide structures in the form of streamwise rolls that exist in turbulent Couette flows. Such structures are coherent regions of either positive or negative streamwise velocity fluctuations. They have been observed both experimentally (Tillmark 1995; Kitoh, Nakabyashi & Nishimura 2005) and numerically (Bech *et al.* 1995; Komminaho, Lundbladh & Johansson 1996; Tsukahara, Kawamura & Shingai 2006; Pirozzoli, Bernardini & Orlandi 2011; Bernardini, Pirozzoli & Orlandi 2013; Avsarkisov *et al.* 2014; Pirozzoli, Bernardini & Orlandi 2014), persisting even if the flow is influenced by a cross-flow (Kraheberger, Hoyas & Oberlack 2018) or a streamwise pressure gradient (Gandía-Barberá *et al.* 2018). Lee & Moser (2018) obtained structures at least as long as $310h$ for $Re_\tau = 500$. On the other hand, Gandía Barberá *et al.* (2021) has shown that stratification processes in thermoconvective flows can effectively remove them.

In a recently published theoretical work by Dokoza & Oberlack (2023) on the roll-cell structures in turbulent Couette flow, these structures are analysed for large longitudinal extension ($\alpha \to 0$), where α represents the wavenumber in streamwise direction, in the limit of large Reynolds numbers. Therein, based on the resolvent analysis, the authors show that in the distinguished limit $\alpha \to 0$ and $Re \to \infty$, where Re here, unlike Re_τ, is based on the bulk velocity, the product $Re\alpha = O(1)$ delivers invariant structures, and, as a result, the rolls grow with increasing Reynolds number. The original idea goes back to an analysis by Yalcin, Turkac & Oberlack (2021), who showed the corresponding invariance for the Orr–Sommerfeld equation.

For Poiseuille flow, Lozano-Durán & Jiménez (2014) noticed that even relatively small computational boxes of streamwise and spanwise sizes of only $2\pi h \times \pi h$ can satisfactorily recover the one-point statistics of the flow. Lluesma-Rodríguez, Hoyas & Peréz-Quiles (2018) also proved a similar result, considering the energy equation. However, this is a controversial point in the Couette flow case. As mentioned, the long and wide structures can be as long as the computational box itself (Lee & Moser 2018). Consequently, a wide range of dimensions of the computational box has been studied. Table 1 contains the most

Work	Re_τ	$L_x/(\pi h)$	$L_z/(\pi h)$	Δx^+	Δy^+	Δz^+
Tsukahara *et al.* (2006)	126	14	4	11.03	0.18–5.67	6.31
	126	20	2	7.88	0.18–5.67	5.90
Avsarkisov *et al.* (2014)	125–550	20	6	13	0.92–5.9	6.5
Pirozzoli *et al.* (2014)	171–986	18	8	7	0.08–8.8	5
Lee & Moser (2018)	93–501	100	5	10.25	0.040–6.33	5.13
Kraheberger *et al.* (2018)	250–1000	8	3	12.2	0.42–7.2	6.13
Gandía-Barberá *et al.* (2018)	132	128	6	9.4	0.83–2.3	4.7
Alcántara-Ávila, Barberá & Hoyas (2019)	180–500	16	6	8.4	0.83–2.3	4.3
Gandía Barberá *et al.* (2021)	480	8	3	8.2	0.83–2.3	4.1

Table 1. Most relevant publications of DNS of plane Couette flow. The second column shows the ranges of Re_τ simulated for the dimensions of the computational box shown in columns three and four. The last three columns show the mesh resolution.

relevant publications of Couette flow studies, together with Re_τ, the computational box dimensions and the mesh resolution.

The most crucial point about these rolls is that they can significantly influence the flow statistics (Alcántara-Ávila *et al.* 2019). In that work, the authors performed several simulations of a turbulent Couette flow at $Re_\tau = 180$ with different spanwise sizes, ranging from $\pi/2h$ to $6\pi h$. They found that the number of velocity rolls does not affect the mean flow. However, intensities are greatly affected, mainly in the centre of the channel. Thus, a wide computational box that can accommodate several rolls is needed to simulate the flow accurately.

Our present study aims to analyse the kinematics of Couette flow at a larger Reynolds number, up to $Re_\tau = 2000$ in a wide and long box. We found that it is possible that the rolls are not as large as previously thought. Roll length can be again finite for this friction Reynolds number. Apart from that, particular emphasis will be given to several points raised recently in Poiseuille flows, including the value of the von Kármán constant, the scaling of the intensity of the streamwise velocity and the scaling of the dissipation (Hoyas *et al.* 2022).

2. Numerical methods and simulations

This work presents two new simulations for friction Reynolds numbers $Re_\tau = 1000$ and $Re_\tau = 2000$. Both computations have been performed within a computational box of $L_x = 16\pi h$, $L_y = 2h$ and $L_z = 6\pi h$ with spanwise and streamwise periodicities. The streamwise, wall-normal and spanwise coordinates are x, y and z and the corresponding instantaneous velocity components are U, V and W, respectively. Defining the space–time average operator $\langle\cdot\rangle_{x_i}$ as

$$\langle\phi\rangle_{x_i} = \frac{1}{L_{x_i}(t_1 - t_0)} \int_{t_0}^{t_1} \int_0^{L_{x_i}} \phi \, \mathrm{d}x_i \, \mathrm{d}t. \tag{2.1}$$

The value of $\langle\phi\rangle_x$ can be thought as the mean in x of the time-averaged field ϕ. Statistically averaged quantities in x and z are denoted by an overbar, $\bar{\phi} = \langle\phi\rangle_{xz}$, whereas fluctuating quantities are denoted by lowercase letters, i.e. $U = \langle U\rangle_{xz} + u = \bar{U} + u$. Primes are reserved for intensities: $u' = \overline{uu}^{1/2}$.

The numerical methods of the two new DNS are based on those described by Kim *et al.* (1987). A similar algorithm, including the energy equation, is described in

Case	Line style	Re_τ	L_x/h	L_z/h	Δx^+	Δz^+	N_x	N_y	N_z	$u_\tau T/h$	ε	$\max(u'^+)$
C2000	———	2007	16π	6π	8.17	3.06	12 288	633	9216	13.4	8×10^{-4}	3.17
C1000	- ◇ -	1034	16π	6π	8.17	3.06	6144	383	4608	25.72	2×10^{-3}	3.16
C986	- ○ -	986	18π	8π	6.80	4.84	8192	512	5120	54.1	1×10^{-3}	3.15
C550	- ⊕ -	551	20π	6π	8.88	4.5	3888	251	2304	57	3×10^{-4}	3.06
C500	- □ -	501	100π	5π	10.25	5.13	15 360	256	1536	150	4×10^{-4}	3.12

Table 2. Summary of the simulations discussed. Here L_x and L_z are the numerical box's periodic streamwise and spanwise dimensions; h is the channel half-height; Δx^+ and Δz^+ are the resolutions in terms of dealiased Fourier modes; N_x, N_y, N_z are the numbers of collocation points. The time span of the simulation is given in terms of eddy turnovers $u_\tau T/h$, where T is the computational time; ε is a measure of convergence, defined in Vinuesa *et al.* (2016). The maximum of u'^+ is given in the last column. Line styles given in the second column are used throughout the paper. Data references are C986 Pirozzoli *et al.* (2014), C550 Avsarkisov *et al.* (2014) and C500 Lee & Moser (2018).

Lluesma-Rodríguez *et al.* (2021). These algorithms were implemented under a code name LISO that was validated for Poiseuille flows in Hoyas & Jiménez (2006) and for Couette flows in Avsarkisov *et al.* (2014). This code is highly parallelizable, including the input/output operations, allowing high-resolution simulations (Yousif *et al.* 2023) or high-demanding computational power (Hoyas *et al.* 2022).

Table 2 summarizes the parameters of all the Couette flow simulations used in this paper. Information about the two new cases described above, namely C1000 and C2000, are given in the first two rows. The wall-normal grid spacing of these two cases is adjusted to keep the resolution $\Delta y \cong 1.5\eta$ approximately constant in terms of the local Kolmogorov scale $\eta = (\nu^3/\varepsilon)^{1/4}$. Using wall units, Δy^+ varies from 0.32 at the wall to $\Delta y^+ \simeq 8.9$ at the centreline.

The running times given in table 2 are provided regarding eddy turnover time units, $u_\tau T/h$. The initial file of these simulations was taken from a smaller Reynolds number simulation. In particular, the initial file for the C2000 simulation was taken from the C1000. The table does not include the transition until a statistically steady state is reached. One of the tools used to assert whether such a statistically steady state has been reached is to compute the total shear stress, figure 2(*a*). This stress should equal 1 in Couette flows, as integration and non-dimensionalization of the x-component of the mean momentum equation (Avsarkisov *et al.* 2014) yields

$$1 = \frac{\mathrm{d}\bar{U}^+}{\mathrm{d}y^+} - \overline{uv}^+. \tag{2.2}$$

The parameter ε is defined as the L2 norm of the difference between the two sides of (2.2) (Vinuesa *et al.* 2016). This difference is below 3×10^{-3} in all cases, as shown in figure 2(*b*). The ε value in table 2 indicates that the simulation statistics have converged. Notice that every simulation follows this convergence criterion, due to the mesh sizes being similar. This is remarkable as Pirozzoli *et al.* (2014), and Lee & Moser (2018) use a different method from LISO.

We have also computed a bound for the error of the statistics as in Hoyas & Jiménez (2008). While the standard deviation of the data is below 0.4 % for $\bar{U}$, it is considerably larger, up to 7 %, for the intensities. As explained later, this is an effect of the very large structures of the flow. As the number of samples is 85 000, the standard error is below 0.1 % in every statistic presented.

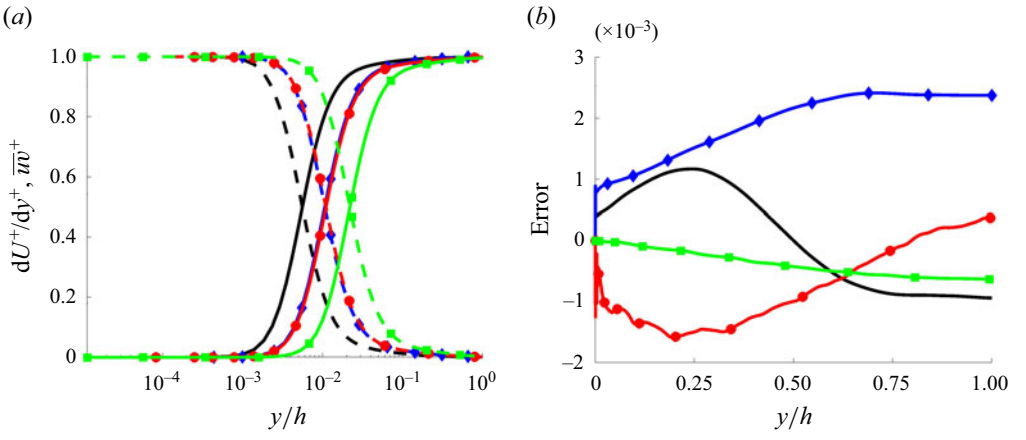

Figure 2. Lines as in table 2. (*a*) Shear and Reynolds stress: $\mathrm{d}\bar{U}^+/\mathrm{d}y^+$ (dash-dot), $\overline{uv}^+$ (solid). Symbols as given in table 2. Notice how the two cases at $Re_\tau = 1000$ are basically the same. (*b*) Difference between left-hand side and right-hand side of (2.2).

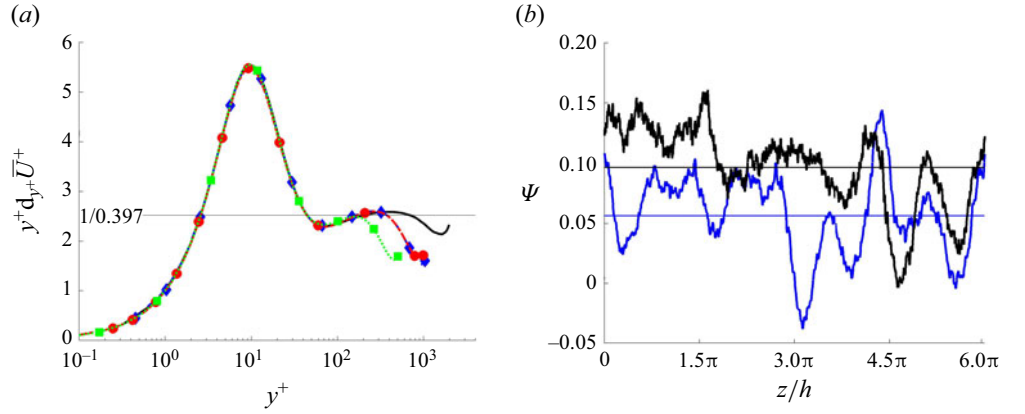

Figure 3. Lines as in table 2. (*a*) Indicator function for the different cases. The agreement is excellent for the 1000 cases. (*b*) Evolution in z of the values of Ψ. The straight lines are the average of the cases.

3. DNS results

3.1. *Mean velocity*

The mean velocity profile is shown in figure 3(*a*) in terms of the indicator function, $\Gamma = y^+\partial_{y^+}\bar{U}^+$. This function shows a plateau if the scaling for the logarithmic layer $\bar{U}^+ = \kappa^{-1}\log(y^+) + B$ holds, where κ is the von Kármán constant (Oberlack *et al.* 2022) and B is the interception constant.

The thin solid line represents the classical logarithmic law of the wall for a von Kármán constant $\kappa = 0.397$, the value obtained for the C2000 simulation. For the case C1000, a value of $\kappa = 0.41$ fits the data a bit better, while in previous Couette simulations, the following values were obtained: $\kappa = 0.41$ (Pirozzoli *et al.* 2014), $\kappa = 0.41$ (Avsarkisov *et al.* 2014) and $\kappa = 0.384$ (Lee & Moser 2018). A constant region, such as that appearing in Hoyas *et al.* (2022), is not observed for any cases, including C2000. As expected (Lee & Moser 2015), even the highest Reynolds number presented here seems too low to produce

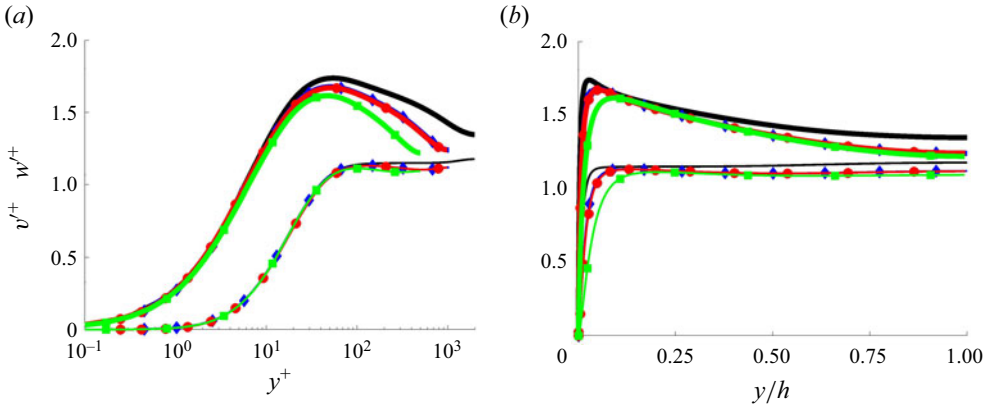

Figure 4. Lines as in table 2. Thin lines: v'^+. Thick lines: w'^+. The y scale is wall units y^+ (a) and outer units y/h (b).

a sufficiently long log layer (Monkewitz 2021; Hoyas *et al.* 2022), that would probably start at approximately $y^+ \approx 300$.

An open question in Couette flows is if the value of the non-dimensional velocity gradient at the channel centreline, sometimes called the slope parameter, is zero for an infinite Reynolds number. This parameter is defined as in Avsarkisov *et al.* (2014),

$$\Psi = \frac{h}{U_w}\frac{\mathrm{d}U}{\mathrm{d}y}\bigg|_{cl} \tag{3.1}$$

This value has been discussed in several works. Reichardt (1959) and Busse (1970) determined a value of $\Psi = 0.25$ at infinite Reynolds number, while Lund & Bush (1980) performed an asymptotic analysis and concluded that it approaches zero as $Re \to \infty$. In our case, however, we find $\Psi_{1000} = 0.066$ and $\Psi_{2000} = 0.097$, which are in line with the results of Lee & Moser (2018). Hence, as $\Psi_{2000} > \Psi_{1000}$, this may indicate a change of tendency or a hint of the difficulty of accurately computing statistics on the outer flow due to the existence of very large structures, see figure 3(b). This figure shows the value of Ψ evaluated after averaging 100 images of the flow. The mean of Ψ is basically the same as that computed with the whole database, but the differences across z are very high, probably due to the large structures of the flow. Finally, as Ψ involves wall-normal derivatives, a very long time for computing accurate statistics should be expected (Hoyas *et al.* 2024).

3.2. *Velocity fluctuations*

Neither v'^+ or w'^+ collapses exactly in wall units, see figure 4(a). As in Poiseuille flows (Hoyas *et al.* 2022), the maximum of these intensities is still growing with Re_τ. The value of v'^+ is remarkably similar to that predicted for Poiseuille flows in Spalart & Abe (2021). However, there seems to be a greater dispersion in the value in the channel centre figure 4(b), with the C2000 case being rather different. A simulation at a larger Reynolds number seems necessary to elucidate if this is a change of tendency or, again, an effect of the structures (Alcántara-Ávila, Hoyas & Pérez-Quiles 2018).

The intensity of u, u', is shown in figure 5(a). Close to the wall, the peak of the u'^+ does not seem to increase appreciably with the Reynolds number but reaches a finite value (last column of table 2). These numbers are appreciably larger than that of Hoyas *et al.*

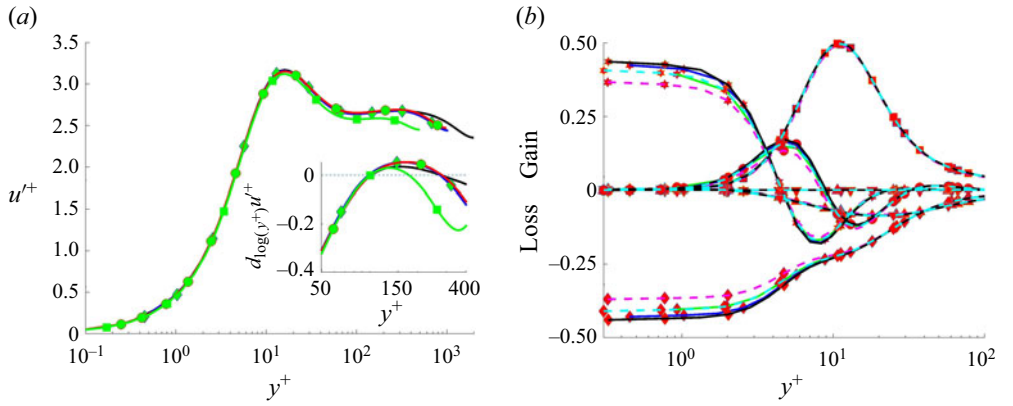

Figure 5. Lines as in table 1. (*a*) u'^+. Inset: derivative of u'^+ for y^+ close to the second maximum. (*b*) Budgets for Reynolds stresses in wall units for u'. Production ■, dissipation ♦, viscous diffusion ∗, pressure strain ▼, pressure diffusion ▲, turbulent diffusion •. Purple and cyan dashed lines, Poiseuille channel at $Re_\tau = 2000$ (Hoyas *et al.* 2022) and $Re_\tau = 10\,000$ (Hoyas & Jiménez 2006), respectively.

(2022) for $Re_\tau = 10\,000$, $\max(u'^+) = 3.07$. Several experimental (Hultmark *et al.* 2012; Willert *et al.* 2017) and theoretical studies (Chen & Sreenivasan 2021) suggested that this limit could be bounded in wall turbulence. Furthermore, this limit does not depend on the channel length, as Lee and Moser (2018) found for $Re_\tau = 500$ and $L_x = 100\pi h$. This boundness is a remarkable difference between Couette and pressure-driven flows, as this maximum grows without bound in the range of Reynolds numbers described up to now (Marusic, Baars & Hutchins 2017; Hoyas *et al.* 2022). The second maximum in u'^+, at approximately $y^+ = 270$, appears at a Reynolds number far smaller than in Poiseuille channels (Hoyas *et al.* 2022) or boundary layers (Samie *et al.* 2018).

The agreement between Couette and Poiseuille flows is remarkably good in wide regions of the turbulent budget terms of $\overline{u_i u_i}$:

$$B^s_{ij} \equiv \frac{\mathrm{D}\overline{u_i u_j}}{\mathrm{D}t} = P_{ij} + \varepsilon_{ij} + T_{ij} + \Pi^s_{ij} + \Pi^d_{ij} + V_{ij}, \tag{3.2}$$

where $\mathrm{D}/\mathrm{D}t$ is the mean substantial derivative. The terms on the right-hand side are production, dissipation, turbulent diffusion, pressure strain, pressure diffusion and viscous diffusion. The exact definition of these terms can be found in Hoyas & Jiménez (2008) and Avsarkisov *et al.* (2014). For the sake of brevity, we will only discuss B_{11} here. For the other cases, see the availability statement about the data. Figure 5(*b*) presents data for Couette (solid lines) and Poiseuille (dashed lines). The Couette cases follow the same colour code as in table 2. The two Poiseuille channels are at $Re_\tau = 2000$ (magenta) (Hoyas & Jiménez 2006) and $Re_\tau = 10\,000$ (purple) (Hoyas *et al.* 2022). The first conclusion is that the scaling is perfect for all cases above $y^+ \approx 10$. The peak of the production term at $y^+ \approx 12$ can be considered universal.

A second point is the anomalous scaling of the dissipation (Hoyas & Jiménez 2008). As it is well known, the dissipation does not collapse in wall units for the Poiseuille cases (Hoyas *et al.* 2022). This situation changes for Couette flow. As shown in figure 5(*b*), the dissipation value at the wall is almost constant, with a value of $(\mathrm{d}/\mathrm{d}y)u'^+|_{y^+=0} = 0.4665$ and 0.4653 for C1000 and C2000, respectively. This behaviour can be linked to the finite value of the maximum of u'^+ (Alcántara-Ávila, Hoyas & Pérez-Quiles 2021; Hoyas *et al.* 2022).

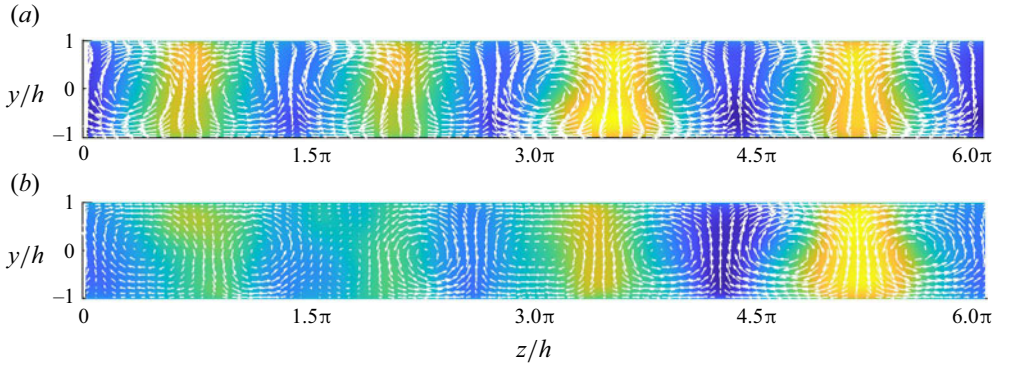

Figure 6. The x-averaged field $\langle u\rangle_x$. The value of the vector field $(\langle v\rangle_x, \langle w\rangle_x)$ is represented with arrows. (a) C1000 case. (b) C2000 case.

3.3. *Superstructures in Couette flows*

As stated above, the most remarkable difference between Couette and Poiseuille flows is the existence of very long rolls with a width of approximately $\delta \approx 6/8\pi h$.

The footprints of these structures fill the whole channel, as shown in figure 6. Here, we have plotted the x-average of the streamwise fluctuation, $\langle u\rangle_x$, as the background colour. The value of the vector field $(\langle v\rangle_x, \langle w\rangle_x)$ is represented with arrows. As we can see, it is possible to identify four structures with a width of $\ell_z \approx 6/8\pi h$, approximately. This width is similar to the previous ones reported (Lee & Moser 2018). The length of these structures can be obtained by studying the correlation in x of u:

$$R_x(s) = \frac{\langle u(x, y, z)u(x + s, y, z)\rangle}{u'^2}, \quad R_z(s) = \frac{\langle u(x, y, z)u(x, y, z + s)\rangle}{u'^2}. \tag{3.3a,b}$$

This correlation is shown at the channel centre, figure 7(a,b). The white lines mark the boundary among the rolls. Lee & Moser (2018) showed that for $Re_\tau = 500$, the structures were extremely long, with a length of at least $100h$. Alcántara-Ávila *et al.* (2019) obtained a similar result for thermal Couette flow. Our results offer a different trend than the previous results at smaller Reynolds numbers. In the C1000 case, the correlation is large for the four structures, filling the entire box length, while the structures of the C2000 case from $z/h = 0$ to 3π are smaller than the box. This can be appreciated better in figure 7(c). Here, the value of R_x can be seen at $\ell_x = 6\pi h$. The maximum of this correlation is always greater than 0.3 for the C1000 case, but it is negative in some z/h points for the C2000 case, indicating that the length of the coherent structure is less than ℓ_x. Therefore, some parts of the channel can keep very large rolls, while in other regions, these rolls are limited to lengths below $\ell_x = 6\pi h$. This is a new effect that has not been reported for turbulent Couette flow and points to the uncertainty that is observed for certain statistical quantities, such as the slope parameter ψ in (3.1).

4. Conclusions

This paper presents two simulations at two different friction Reynolds numbers, namely 1000 and 2000. The simulations were carried out in a very large box of size $L_x = 16\pi h$, $L_y = 2h$ and $L_z = 6\pi h$. For the C2000 case, a clear log layer is only observed in parts. Through a fitting, a value of $\kappa = 0.397$ has been obtained. This value is a bit higher than Poiseuille channels and similar to other Couette ones. The scaling of the intensities is

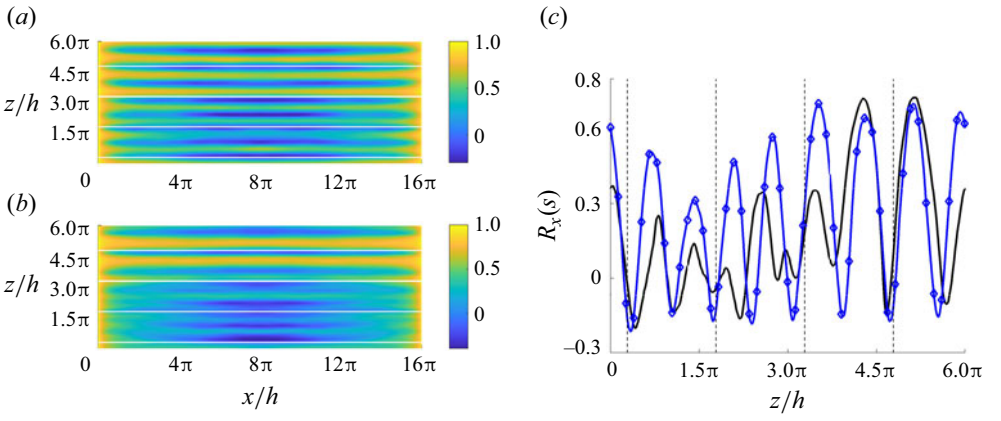

Figure 7. (*a*,*b*) $R_x(s)$ for C1000 (*a*) and C2000 (*b*). In both figures, we have added $\langle\phi\rangle_x$, showing the size in z of the pair of rolls. (*c*) $R_x(s)$ at $\ell_x = 6\pi h$. The different rolls are marked using a dashed vertical line.

perfect in the buffer layer and below. The first maximum of u'^+ does not grow anymore, and a second maximum has clearly appeared at $y^+ \approx 350$. This value is similar to that expected for Poiseuille channels (Hoyas *et al.* 2022), but at a far lower Reynolds number. The scaling failure of the dissipation is also not present anymore. This can be traced to the constant value of $(\mathrm{d}/\mathrm{d}y)u'^+$ at the wall.

The intensities of the C2000 case are remarkably different from those at lower Reynolds numbers at the channel centre. This is probably due to the organization of the large scales of u. These large scales were thought to be almost infinite. We obtained the same result for the C1000 case. However, for the C2000 case, some rolls present a finite size with a length of approximately $\ell_x = 6\pi$. The width of every roll is approximately $\ell_z = 6/8\pi$. Simulations at a larger Reynolds number are needed to elucidate if these structures are bounded.

Funding. The authors gratefully acknowledge the provision of computing time on the Gauss Centre for Supercomputing e.V. on the GCS Supercomputer SuperMUC-NG at Leibniz Supercomputing Centre under project number pr92la. M.O. acknowledges partial funding by the German Research Foundation (DFG) under the project OB 96/48-1. S.H. is partially funded by project PID2021-128676OB-I00 by Ministerio de Ciencia, innovación y Universidades/FEDER.

Declaration of interests. The authors report no conflict of interest.

Author ORCIDs.
Sergio Hoyas https://orcid.org/0000-0002-8458-7288;
Martin Oberlack https://orcid.org/0000-0002-5849-3755.

References

Alcántara-Ávila, F., Barberá, G. & Hoyas, S. 2019 Evidences of persisting thermal structures in Couette flows. *Intl J. Heat Fluid Flow* **76**, 287–295.

Alcántara-Ávila, F., Hoyas, S. & Pérez-Quiles, M.J. 2018 DNS of thermal channel flow up to $Re_\tau = 2000$ for medium to low Prandtl numbers. *Intl J. Heat Mass Transfer* **127**, 349–361.

Alcántara-Ávila, F., Hoyas, S. & Pérez-Quiles, M.J. 2021 Direct numerical simulation of thermal channel flow for $Re_\tau = 5000$ and $Pr = 0.71$. *J. Fluid Mech.* **916**, A29.

Avsarkisov, V., Hoyas, S., Oberlack, M. & García-Galache, J.P. 2014 Turbulent plane Couette flow at moderately high Reynolds number. *J. Fluid Mech.* **751**, R1.

Bech, K., Tillmark, N., Alfredsson, P. & Andersson, H. 1995 An investigation of turbulent plane Couette flow at low Reynolds numbers. *J. Fluid Mech.* **286**, 291–325.

BERNARDINI, M., PIROZZOLI, S. & ORLANDI, P. 2013 The effect of large-scale turbulent structures on particle dispersion in wall-bounded flows. *Intl J. Multiphase Flow* **51**, 55–64.

BUSSE, F.H. 1970 Bounds for turbulent shear flow. *J. Fluid Mech* **41**, 219–240.

CHEN, X. & SREENIVASAN, K.R. 2021 Reynolds number scaling of the peak turbulence intensity in wall flows. *J. Fluid Mech.* **908**, R3.

DOKOZA, T. & OBERLACK, M. 2023 Reynolds number induced growth of the large-scale rolls in plane Couette flow using resolvent analysis. *J. Fluid Mech.* **968**, A23.

GANDÍA BARBERÁ, S., ALCÁNTARA-ÁVILA, F., HOYAS, S. & AVSARKISOV, V. 2021 Stratification effect on extreme-scale rolls in plane Couette flows. *Phys. Rev.* E **6**, 034605.

GANDÍA-BARBERÁ, S, HOYAS, S., OBERLACK, M & KRAHEBERGER, S.V. 2018 The link between the Reynolds shear stress and the large structures of turbulent Couette-Poiseuille flow. *Phys. Fluids* **30** (4), 041702.

HOYAS, S., BAXERRES, V., NAGIB, H. & VINUESA, R. 2024 Resolution and convergence requirements for extended overlap region in wall-bounded turbulence. *Phys. Rev. Fluids* (submitted).

HOYAS, S. & JIMÉNEZ, J. 2006 Scaling of the velocity fluctuations in turbulent channels up to $Re_\tau = 2003$. *Phys. Fluids* **18** (1), 011702.

HOYAS, S. & JIMÉNEZ, J. 2008 Reynolds number effects on the Reynolds-stress budgets in turbulent channels. *Phys. Fluids* **20** (10), 101511.

HOYAS, S., OBERLACK, M., ALCÁNTARA-ÁVILA, F., KRAHEBERGER, S.V. & LAUX, J. 2022 Wall turbulence at high friction Reynolds numbers. *Phys. Rev. Fluids* **7**, 014602.

HULTMARK, M., VALLIKIVI, M., BAILEY, S.C.C. & SMITS, A.J. 2012 Turbulent pipe flow at extreme Reynolds numbers. *Phys. Rev. Lett.* **108**, 094501.

KIM, J., MOIN, P. & MOSER, R. 1987 Turbulence statistics in fully developed channels flows at low Reynolds numbers. *J. Fluid Mech.* **177**, 133–166.

KITOH, O., NAKABYASHI, K. & NISHIMURA, F. 2005 Experimental study on mean velocity and turbulence characteristics of plane Couette flow: low-Reynolds-number effects and large longitudinal vortical structure. *J. Fluid Mech.* **539**, 199–227.

KOMMINAHO, J., LUNDBLADH, A. & JOHANSSON, A. 1996 Very large structures in plane turbulent Couette flow. *J. Fluid Mech.* **320**, 259–285.

KRAHEBERGER, S., HOYAS, S. & OBERLACK, M. 2018 DNS of a turbulent Couette flow at constant wall transpiration up to $Re_\tau = 1000$. *J. Fluid Mech.* **835**, 421–443.

LEE, M. & MOSER, R. 2015 Direct numerical simulation of turbulent channel flow up to $Re_\tau \approx 5200$. *J. Fluid Mech.* **774**, 395–415.

LEE, M. & MOSER, R. 2018 Extreme-scale motions in turbulent plane Couette flows. *J. Fluid Mech.* **842**, 128–145.

LLUESMA-RODRÍGUEZ, F., ÁLCANTARA ÁVILA, F., PÉREZ-QUILES, M.J. & HOYAS, S. 2021 A code for simulating heat transfer in turbulent channel flow. *Mathematics* **9** (7), 756.

LLUESMA-RODRÍGUEZ, F., HOYAS, S. & PERÉZ-QUILES, M.J. 2018 Influence of the computational domain on DNS of turbulent heat transfer up to $Re_\tau = 2000$ for $Pr = 0.71$. *Intl J. Heat Mass Transfer* **122**, 983–992.

LOZANO-DURÁN, A. & JIMÉNEZ, J. 2014 Effect of the computational domain on direct simulations of turbulent channels up to $Re_\tau = 4200$. *Phys. Fluids* **26** (1), 011702.

LUND, K.O. & BUSH, W.B. 1980 Asymptotic analysis of plane turbulent Couette-Poiseuille flows. *J. Fluid Mech.* **96** (1), 81–104.

MARUSIC, I., BAARS, W.J. & HUTCHINS, N. 2017 Scaling of the streamwise turbulence intensity in the context of inner-outer interactions in wall turbulence. *Phys. Rev. Fluids* **2**, 100502.

MONKEWITZ, P.A. 2021 The late start of the mean velocity overlap log law at-a generic feature of turbulent wall layers in ducts. *J. Fluid Mech.* **910**, A45.

OBERLACK, M., HOYAS, S., KRAHEBERGER, S.V., ALCÁNTARA-ÁVILA, F. & LAUX, J. 2022 Turbulence statistics of arbitrary moments of wall-bounded shear flows: a symmetry approach. *Phys. Rev. Lett.* **128**, 024502.

PIROZZOLI, S., BERNARDINI, M. & ORLANDI, P. 2011 Large-scale motions and inner/outer layer interactions in turbulent Couette–Poiseuille flows. *J. Fluid Mech.* **680**, 534–563.

PIROZZOLI, S., BERNARDINI, M. & ORLANDI, P. 2014 Turbulence statistics in Couette flow at high Reynolds number. *J. Fluid Mech.* **758**, 323–343.

REICHARDT, H. 1959 *Gezetzmässigkeiten der geradlinigen turbulenten Couetteströmung* [in German]. Mitteilungen aus dem Max-Planck-Institut für Strömungsforschung Göttingen 22.

SAMIE, M., MARUSIC, I., HUTCHINS, N., FU, M.K., FAN, Y., HULTMARK, M. & SMITS, A.J. 2018 Fully resolved measurements of turbulent boundary layer flows up to $Re_\tau = 20\,000$. *J. Fluid Mech.* **851**, 391–415.

SPALART, P.R. & ABE, H. 2021 Empirical scaling laws for wall-bounded turbulence deduced from direct numerical simulations. *Phys. Rev. Fluids* **6** (4), 044604.

TILLMARK, N. 1995 Experiments on transition and turbulence in plane Couette flow. PhD thesis, KTH, Royal Institute of Technology.

TSUKAHARA, T., KAWAMURA, H. & SHINGAI, K. 2006 DNS of turbulent Couette flow with emphasis on the large-scale structure in the core region. *J. Turbul.* **7**, 1–16.

VINUESA, R., PRUS, C., SCHLATTER, P. & NAGIB, H. 2016 Convergence of numerical simulations of turbulent wall-bounded flows and mean cross-flow structure of rectangular ducts. *Meccanica* **51**, 3025–3042.

WILLERT, C.E., *et al.* 2017 Near-wall statistics of a turbulent pipe flow at shear Reynolds numbers up to 40 000. *J. Fluid Mech.* **826**, R5.

YALCIN, A., TURKAC, Y. & OBERLACK, M. 2021 On the temporal linear stability of the asymptotic suction boundary layer. *Phys. Fluids* **33** (5), 054111.

YOUSIF, M.Z., YU, L., HOYAS, S., VINUESA, R. & LIM, H.C. 2023 A deep-learning approach for reconstructing 3d turbulent flows from 2d observation data. *Sci. Rep.* **13** (1), 2529.